

**DYNAMICAL SYSTEM STUDY OF THE
HODGKIN-HUXLEY, FITZHUGH-NAGUMO
AND MORRIS-LECAR MODELS OF
NERVE MEMBRANES**

NUR SHAFIKA ABEL BINTI RAZALI

**UNIVERSITI SAINS MALAYSIA
2019**

**DYNAMICAL SYSTEM STUDY OF THE
HODGKIN-HUXLEY, FITZHUGH-NAGUMO
AND MORRIS-LECAR MODELS OF
NERVE MEMBRANES**

by

NUR SHAFIKA ABEL BINTI RAZALI

**Thesis submitted in fulfilment of the requirements
for the degree of
Doctor of Philosophy**

May 2019

ACKNOWLEDGEMENT

Alhamdulillah, I manage to complete my thesis with fully understanding and finally found what I have been searching during my Ph.D journey; treasure His unique and perfect creation.

Firstly, I would like to express my sincere gratitude to my supervisor, Associate Professor Dr. Farah Aini Binti Abdullah for the continuous support of my Ph.D study and related research, for her patience, motivation and immense knowledge. Her guidance helped me in all the time of research and writing of this thesis. I could not have imagined having a better supervisor and mentor for my Ph.D study.

Besides my supervisor, I would like to thank Dr. Mohd Hafiz Bin Mohd for his insightful comments and encouragement.

I am forever grateful to my family, without them I would not be who and where I am today.

TABLE OF CONTENTS

Acknowledgement	ii
Table of Contents	iii
List of Tables	vii
List of Figures	viii
List of Abbreviations	xvii
List of Symbols	xix
Abstrak	xxiii
Abstract	xxv
CHAPTER 1 – INTRODUCTION	
1.1 Preliminary	1
1.2 Mechanism of Single Neuron	2
1.2.1 Resting Potential	4
1.2.2 Action Potential	4
1.3 Theoretical and Concept of Dynamical System	6
1.3.1 Dynamical Systems	6
1.3.2 Orbits	8
1.3.3 Phase Portrait	9
1.3.4 Infinitesimal Generator	10
1.3.5 Fixed Points and Equilibrium Solutions	12
1.3.6 Cycles and Periodic Solutions	14
1.3.7 Lyapunov Stability	16
1.3.8 Bifurcation	20
1.3.8 (a) Codimension One Bifurcation (Curves)	21

1.3.8 (b)	Codimension Two Bifurcation (Points)	22
1.4	Motivation	22
1.5	Problem Statements	25
1.6	Research Objectives	26
1.7	Thesis Organization	28
CHAPTER 2 – LITERATURE REVIEW AND MODELS OF NERVE MEMBRANES		
2.1	Introduction	31
2.2	Literature Review	32
2.2.1	Hodgkin-Huxley Model	32
2.2.2	FitzHugh-Nagumo Model	35
2.2.3	Morris-Lecar Model	37
2.3	Derivation of the Nerve Membranes Models	39
2.3.1	4-Differential HH Equations and Parameters	39
2.3.2	2-Differential FHN Equations and Parameters	45
2.3.3	2-Differential ML Equation and Parameters	52
2.4	Regenerated Dynamical Analysis	54
2.4.1	Regenerated Dynamical Analysis of the HH Model	54
2.4.2	Regenerated Dynamical Analysis of the FHN Model	56
2.4.3	Regenerated Dynamical Analysis of the ML Model	59
2.5	Numerical Package for Continuation and Bifurcation Analysis: XPPAut and MatCont	63
2.5.1	Computational in XPPAut	64
2.5.2	Bifurcation and Continuation by AUTO	67
2.5.3	Codimension of Bifurcation in MatCont	69

2.5.4	Computational in MatCont	71
2.6	Summary	74
CHAPTER 3 – DYNAMICS OF THE HODGKIN-HUXLEY EQUATIONS		
3.1	Introduction	75
3.2	Numerical Detection	75
3.3	One-Parameter Bifurcation Analysis for HH Model	76
3.4	Two-Parameters Bifurcation Analysis for HH Model	82
3.5	Reasonable Range of Each Bifurcation Parameters in HH Model	89
3.6	Discussion	90
CHAPTER 4 – DYNAMICS OF THE FITZHUGH-NAGUMO EQUATIONS		
4.1	Introduction	92
4.2	Numerical Detection	92
4.3	One-Parameter Bifurcation Analysis for FHN Model	93
4.4	Two-Parameters Bifurcation Analysis for FHN Model	96
4.5	Reasonable Range of Each Bifurcation Parameters in FHN Model	99
4.6	Discussion	99
CHAPTER 5 – DYNAMICS OF THE MORRIS-LECAR EQUATIONS		
5.1	Introduction	102
5.2	Numerical Detection	102
5.3	One-Parameter Bifurcation Analysis for ML Model	103
5.4	Two-Parameters Bifurcation Analysis for ML Model	108
5.5	Reasonable Range of Each Bifurcation Parameters in ML Model	116
5.6	Discussion	116

CHAPTER 6 – CONCLUSION AND FUTURE WORK

6.1	Summary and Contribution	121
6.2	Limitations of Research	126
6.3	Suggestions for Future Work	126

REFERENCES	127
-------------------	------------

LIST OF PUBLICATIONS

LIST OF TABLES

		Page
Table 2.1	Parameters value for components in HH model (Scott, 2002)	44
Table 2.2	Parameters value for components in FHN model (Keener and Sneyd, 1998)	51
Table 2.3	Parameters value for components in ML model (Rinzel and Ermentrout, 1989)	53
Table 2.4	Steady state and cycle related objects and their labels within the GUI	71
Table 6.1	Summary result of dynamical analysis for HH model	123
Table 6.2	Summary result of dynamical analysis for FHN model	124
Table 6.3	Summary result of dynamical analysis for ML model	125

LIST OF FIGURES

		Page
Figure 1.1	The general structure of a neuron (Bear et al., 2007)	2
Figure 1.2	Ion channels function as pores to permit the flux of ions down their electrochemical potential gradient (Marbán, 2002)	3
Figure 1.3	Recording of an AP in an axon following stimulation due to changes in the permeability of the cell membrane to sodium and potassium ions (Lodish et al., 1995)	5
Figure 1.4	Phase portrait of θ in Example 1.2 (Adolfo, 2019)	9
Figure 2.1	Schematic diagram for equivalent electric circuit modelling ionic current flow across nerve cell membrane as described by HH equations	33
Figure 2.2	Schematic diagram for equivalent electrical circuit modelling tunnel-diode nerve model as described by FHN equations (Nagumo et al., 1962)	36
Figure 2.3	Schematic diagram for equivalent electric circuit modelling a patch of space-clamped barnacle sarcolemma as described by ML equations	38
Figure 2.4	The gating variables n , m and h in original HH equation (2.19), using XPPAut, where we set all parameters as in Table 2.1 with the initial values for n , m and h to be 0.3208, 0.0513 and 0.5841, respectively. (A) shows gating variables in time range until 20ms, while (B) shows gating variables when we extend the observation until 100ms	46
Figure 2.5	Gating variables h versus gating variable n with the initial values for n , m and h to be 0.3208, 0.0513 and 0.5841, respectively	47
Figure 2.6	Fast-slow phase plane for fast-slow model with $I = 0\mu\text{A}/\text{cm}^2$ and other parameters as in Table 2.1, showing the intersection of V - and n -nullclines and their trajectories with the initial values $V = 0.66\text{mV}$ and $n = 0.18$	48
Figure 2.7	V_d -nullcline in FHN model in cubic graph, while W -nullcline in FNH model in linear graph with $\alpha = 0.1$, $\varepsilon = 0.1$, $\gamma = 0.25$ and the initial values $V_d = 0.25$ and $W = 1.0$	51

Figure 2.8	Single AP for HH model, using XPPAut when $I = 0\mu\text{A}/\text{cm}^2$ with the initial conditions $V = -0.2828\text{mV}$, $n = 0.3208$, $m = 0.0513$ and $h = 0.5841$. Other parameters were set as in Table 2.1	54
Figure 2.9	Repetitive AP for HH model, using XPPAut when $I = 10\mu\text{A}/\text{cm}^2$ with the initial conditions $V = -0.2828\text{mV}$, $n = 0.3208$, $m = 0.0513$ and $h = 0.5841$. Other parameters were set as in Table 2.1	55
Figure 2.10	One-parameter bifurcation diagram of HH model when parameters set as in Table 2.1, with the initial conditions $V = -0.2828\text{mV}$, $n = 0.3208$, $m = 0.0513$ and $h = 0.5841$ using AUTO. I is a bifurcation parameter. uH denotes a subcritical Hopf bifurcation, sH denotes a supercritical Hopf bifurcation while LPC denotes a limit point bifurcation of cycles	56
Figure 2.11	Single AP for FHN model, using XPPAut when $I_d = 0$, $\alpha = 0.1$, $\varepsilon = 0.1$ and $\gamma = 0.25$ with the initial conditions $V_d = 0.25$ and $W = 1.0$. Other parameters were set as in Table 2.2	56
Figure 2.12	Repetitive AP for FHN model, using XPPAut when $I_d = 1.0$, $\alpha = 0.1$, $\varepsilon = 0.1$ and $\gamma = 0.25$ with the initial conditions $V_d = 0.25$ and $W = 1.0$. Other parameters were set as in Table 2.2	57
Figure 2.13	Phase portrait for the FHN system, when $I_d = 0$, $\alpha = 0.1$, $\varepsilon = 0.1$ and $\gamma = 0.25$ with the initial conditions $V_d = 0.25$ and $W = 1.0$. For these parameter values the system has a stable resting state and is excitable. Intersect at $(0,0)$. Stable steady state with eigenvalues $-0.062499 \pm 0.313996i$	57
Figure 2.14	Phase portrait for the FHN system, when $I_d = 1.0$, $\alpha = 0.1$, $\varepsilon = 0.158$ and $\gamma = 0.25$ with the initial conditions $V_d = 0.25$ and $W = 1.0$. For these parameter values the resting state is unstable and there is a periodic orbit. Intersect at $(0.25753, 1.0301)$. Unstable steady state with eigenvalues $0.121343 \pm 0.280328i$	58
Figure 2.15	One-parameter bifurcation diagram of FHN equations, when $\alpha = 0.1$, $\varepsilon = 0.1$ and $\gamma = 0.25$ with the initial conditions $V_d = 0.25$ and $W = 1.0$ using AUTO. I as the bifurcation parameter. sH1 and sH2 denote supercritical Hopf bifurcation points	59

Figure 2.16	V -nullcline (red curve), while w -nullclines (green curve) in ML model with the initial conditions $V = -60.899\text{mV}$ $w = 0.014873$ when $I = 150\mu\text{A}/\text{cm}^2$	60
Figure 2.17	No AP for ML model, using XPPAut when $I = 0\mu\text{A}/\text{cm}^2$ with the initial conditions $V = -60.899\text{mV}$ and $w = 0.014873$. Other parameters were set as in Table 2.3	60
Figure 2.18	Repetitive AP for ML model, using XPPAut when $I = 150\mu\text{A}/\text{cm}^2$ with the initial conditions $V = -60.899\text{mV}$ and $w = 0.014873$. Other parameters were set as in Table 2.3	61
Figure 2.19	Phase portrait for the ML system, with $V = -60.899\text{mV}$ and $w = 0.014873$ and no applied current $I = 0\mu\text{A}/\text{cm}^2$. For these parameter values the system has a stable resting state and is excitable. Intersect at $(-60.899, 0.014873)$. Stable steady state with eigenvalues $-0.082493 \pm 0.015473i$	61
Figure 2.20	Phase portrait for the ML system, with $V = -60.899\text{mV}$ and $w = 0.014873$ and applied current $I = 150\mu\text{A}/\text{cm}^2$. For these parameter values the resting state is unstable and there is a periodic orbit. Intersect at $(-6.7922, 0.35752)$. Unstable steady state with eigenvalues $0.265114 \pm 0.022151i$	62
Figure 2.21	One-parameter bifurcation diagram of ML equations, when parameters set as in Table 2.3 with the initial conditions $V = -60.899\text{mV}$ and $w = 0.014873$, using AUTO. I as the bifurcation parameter. uH1 and uH2 denote a subcritical Hopf bifurcation	63
Figure 2.22	Screenshot of XPPAut showing the main window, and other optional windows; equations window, initial data window and parameters window	65
Figure 2.23	Screenshot of XPPAut showing the direction fields, nullclines, its fixed point at the intersection of two nullclines and the eigenvalues	66
Figure 2.24	Screenshot of XPPAut showing several methods of available integration in XPPAut	67
Figure 2.25	Screenshot of AUTO showing stability of steady state, where the thick black line represents stable steady state, while thin red line represents unstable steady state	68
Figure 2.26	Screenshot of AUTO showing the maximum and minimum values of the stable periodic solution (green dots), and the	69

	maximum and minimum values of the unstable periodic branch (blue unfilled dots)	
Figure 2.27	The graph of adjacency for steady state and limit cycle bifurcation in MatCont	70
Figure 2.28	Screenshot of Hodgkin-Huxley saved code in diagram directory	72
Figure 2.29	Screenshot of MatCont showing the main window, 2D-plot, starter and integrator windows, including optional windows; numeric and layout windows	72
Figure 3.1	One-parameter bifurcation diagram for equation (2.19) with different values of V_K using AUTO software; (A) $V_K = -12\text{mV}$, (B) $V_K = -20\text{mV}$, (C) $V_K = -60\text{mV}$, (D) $V_K = -80\text{mV}$, (E) $V_K = -120\text{mV}$ and (F) $V_K = -140\text{mV}$, with the initial conditions $V = -0.2828\text{mV}$, $n = 0.3208$, $m = 0.0513$, and $h = 0.5841$. Other parameters were set as in Table 2.1	78
Figure 3.2	One-parameter bifurcation diagram for equation (2.19) with different values of V_{Na} using AUTO software; (A) $V_{Na} = 115\text{mV}$, (B) $V_{Na} = 87\text{mV}$, (C) $V_{Na} = 86\text{mV}$, (D) $V_{Na} = 85.9\text{mV}$, (E) $V_{Na} = 85\text{mV}$ and (F) $V_{Na} = 84\text{mV}$, with the initial conditions $V = -0.2828\text{mV}$, $n = 0.3208$, $m = 0.0513$, and $h = 0.5841$. Other parameters were set as in Table 2.1	79
Figure 3.3	One-parameter bifurcation diagram for equation (2.19) with different values of \bar{g}_K using AUTO software; (A) $\bar{g}_K = 54\text{m}\bar{\mathcal{U}}/\text{cm}^2$, (B) $\bar{g}_K = 53.5\text{m}\bar{\mathcal{U}}/\text{cm}^2$, (C) $\bar{g}_K = 53.2\text{m}\bar{\mathcal{U}}/\text{cm}^2$, (D) $\bar{g}_K = 53\text{m}\bar{\mathcal{U}}/\text{cm}^2$, (E) $\bar{g}_K = 36\text{m}\bar{\mathcal{U}}/\text{cm}^2$ and (F) $\bar{g}_K = 25\text{m}\bar{\mathcal{U}}/\text{cm}^2$, with the initial conditions $V = -0.2828\text{mV}$, $n = 0.3208$, $m = 0.0513$, and $h = 0.5841$. Other parameters were set as in Table 2.1	80
Figure 3.4	One-parameter bifurcation diagram for equation (2.19) with different values of \bar{g}_{Na} using AUTO software; (A) $\bar{g}_{Na} = 200\text{m}\bar{\mathcal{U}}/\text{cm}^2$, (B) $\bar{g}_{Na} = 120\text{m}\bar{\mathcal{U}}/\text{cm}^2$, (C) $\bar{g}_{Na} = 85\text{m}\bar{\mathcal{U}}/\text{cm}^2$, (D) $\bar{g}_{Na} = 84\text{m}\bar{\mathcal{U}}/\text{cm}^2$, (E) $\bar{g}_{Na} = 83\text{m}\bar{\mathcal{U}}/\text{cm}^2$ and (F) $\bar{g}_{Na} = 82\text{m}\bar{\mathcal{U}}/\text{cm}^2$, with the initial conditions $V = -0.2828\text{mV}$, $n = 0.3208$, $m = 0.0513$ and $h = 0.5841$. Other parameters were set as in Table 2.1	81

Figure 3.5	A) Two-parameters bifurcation structure of I versus V_K , while (B) is the magnification near GH1 and (C) is the magnification near GH, for equation (2.19) with different values of V_K using AUTO software, with the initial conditions $V = -0.2828\text{mV}$, $n = 0.3208$, $m = 0.0513$, and $h = 0.5841$. Other parameters were set as in Table 2.1	82
Figure 3.6	(A) Two-parameters bifurcation structure of I versus V_{Na} , while (B) is the magnification near GH1 and (C) is the magnification near GH2, for equation (2.19) with different values of V_{Na} using AUTO software, with the initial conditions $V = -0.2828\text{mV}$, $n = 0.3208$, $m = 0.0513$, and $h = 0.5841$. Other parameters were set as in Table 2.1	83
Figure 3.7	(A) Two-parameters bifurcation structure of I versus \bar{g}_K , while (B) is the magnification near GH1 and (C) is the magnification near GH2 for equation (2.19) with different values of \bar{g}_K using AUTO software, with the initial conditions $V = -0.2828\text{mV}$, $n = 0.3208$, $m = 0.0513$, and $h = 0.5841$. Other parameters were set as in Table 2.1	84
Figure 3.8	(A) Two parameter bifurcation structure of I versus \bar{g}_{Na} , while (B) is the magnification near GH1 and (C) is the magnification near GH2 for equation (2.19) with different values of \bar{g}_{Na} using AUTO software, with the initial conditions $V = -0.2828\text{mV}$, $n = 0.3208$, $m = 0.0513$, and $h = 0.5841$. Other parameters were set as in Table 2.1	85
Figure 3.9	Membrane potential waveforms for stable steady state in blue region when $V_K = -20\text{mV}$ and $I = 250\mu\text{A}/\text{cm}^2$. In this case, the initial conditions are $V = -0.2828\text{mV}$, $n = 0.3208$, $m = 0.0513$, and $h = 0.5841$	86
Figure 3.10	Membrane potential waveforms for bistability of a periodic solution and a steady state in pink region when $V_K = -40\text{mV}$ and $I = 10\mu\text{A}/\text{cm}^2$. In this case, the initial conditions are $V = -0.2828\text{mV}$, $n = 0.3208$, $m = 0.0513$, and $h = 0.5841$	87
Figure 3.11	Membrane potential waveforms for periodic oscillation in red region when $V_K = -60\text{mV}$ and $I = 200\mu\text{A}/\text{cm}^2$. In this case, the initial conditions are $V = -0.2828\text{mV}$, $n = 0.3208$, $m = 0.0513$, and $h = 0.5841$	87
Figure 3.12	Membrane potential waveforms for bistability of periodic solution in green region when $V_K = -100\text{mV}$ and	88

$I = 350\mu\text{A}/\text{cm}^2$. In this case, the initial conditions are $V = -0.2828\text{mV}$, $n = 0.3208$, $m = 0.0513$, and $h = 0.5841$

- Figure 3.13 Membrane potential waveforms for tristability of periodic solutions and a steady state in purple region when $V_{Na} = 86\text{mV}$ and $I = 37.3\mu\text{A}/\text{cm}^2$. In this case, the initial conditions are $V = -0.2828\text{mV}$, $n = 0.3208$, $m = 0.0513$, and $h = 0.5841$ 88
- Figure 3.14 Reasonable parameter range for (A) $V_K = -12\text{mV}$ until -119mV , (B) $V_{Na} = 85.9\text{mV}$ until 170mV , (C) $\bar{g}_K = 25\text{mS}/\text{cm}^2$ until $53.2\text{mS}/\text{cm}^2$ (D) $\bar{g}_{Na} = 84\text{mS}/\text{cm}^2$ until $200\text{mS}/\text{cm}^2$ 90
- Figure 4.1 One-parameter bifurcation diagram for equation (2.25) with different values of γ using AUTO software; (A) $\gamma = 3$, (B) $\gamma = 2.5$, (C) $\gamma = 2$, (D) $\gamma = 1.5$, (E) $\gamma = 0.5$ and (F) $\gamma = 0$, with the initial conditions for V_d and W were set to be $(0.25, 0.1)$, $\varepsilon = 0.5$ and $\alpha = 0.5$. Other parameters were set as in Table 2.2 94
- Figure 4.2 One-parameter bifurcation diagram for equation (2.25) with different values of ε using AUTO software; (A) $\varepsilon = 1.5$, (B) $\varepsilon = 1.2$, (C) $\varepsilon = 1.0$, (D) $\varepsilon = 0.5$, (E) $\varepsilon = 0.1$ and (F) $\varepsilon = 0$, with the initial conditions for V_d and W were set to be $(0.25, 0.1)$, $\gamma = 0.5$ and $\alpha = 0.5$. Other parameters were set as in Table 2.2 95
- Figure 4.3 Two-parameters bifurcation structure of (A) I_d versus γ and (B) I_d versus ε . With the initial conditions for V_d and W were set to be $(0.25, 0.1)$ and $\alpha = 0.5$. Other parameters were set as in Table 2.2 96
- Figure 4.4 Summary of the stability behaviours in I_d versus γ for FHN model. With the initial conditions for V_d and W were set to be $(0.25, 0.1)$, $\varepsilon = 0.5$ and $\alpha = 0.5$. Other parameters were set as in Table 2.2 97
- Figure 4.5 Membrane potential waveforms for stable steady state in blue region when $\gamma = 2.5$ and $I_d = 10$. In this case, the initial conditions are $V_d = 0.25$ and $W = 1.0$ 98
- Figure 4.6 Membrane potential waveforms for periodic solution in red region when $\gamma = 2.5$ and $I_d = 1.5$. In this case, the initial conditions are $V_d = 0.25$ and $W = 1.0$ 98

- Figure 5.1 One-parameter bifurcation diagram for equation (2.28) 104
with different values of V_K using AUTO software;
(A) $V_K = -40\text{mV}$, (B) $V_K = -55\text{mV}$, (C) $V_K = -70\text{mV}$,
(D) $V_K = -100\text{mV}$, (E) $V_K = -750\text{mV}$ and (F) $V_K = -1000\text{mV}$,
with the initial conditions for V and w were set to be
($-60.899\text{mV}, 0.014873$). Other parameters
were set as in Table 2.3
- Figure 5.2 One-parameter bifurcation diagram for equation (2.28) 105
with different values of V_{Ca} using AUTO software;
(A) $V_{Ca} = 195\text{mV}$, (B) $V_{Ca} = 160\text{mV}$, (C) $V_{Ca} = 100\text{mV}$,
(D) $V_{Ca} = 75\text{mV}$, (E) $V_{Ca} = 70\text{mV}$ and (F) $V_{Ca} = 50\text{mV}$,
with the initial conditions for V and w were set to be
($-60.899\text{mV}, 0.014873$). Other parameters
were set as in Table 2.3
- Figure 5.3 One-parameter bifurcation diagram for equation (2.28) 106
with different values of \bar{g}_K using AUTO software; (A)
 $\bar{g}_K = 25 \text{ m}\bar{\mathcal{U}}/\text{cm}^2$, (B) $\bar{g}_K = 23 \text{ m}\bar{\mathcal{U}}/\text{cm}^2$,
(C) $\bar{g}_K = 20 \text{ m}\bar{\mathcal{U}}/\text{cm}^2$, (D) $\bar{g}_K = 15 \text{ m}\bar{\mathcal{U}}/\text{cm}^2$,
(E) $\bar{g}_K = 5.8 \text{ m}\bar{\mathcal{U}}/\text{cm}^2$ and (F) $\bar{g}_K = 4.0 \text{ m}\bar{\mathcal{U}}/\text{cm}^2$,
with the initial conditions for V and w were set to be
($-60.899\text{mV}, 0.014873$). Other parameters were
set as in Table 2.3
- Figure 5.4 One-parameter bifurcation diagram for equation (2.28) 107
with different values of \bar{g}_{Ca} using AUTO software;
(A) $\bar{g}_{Ca} = 6.8 \text{ m}\bar{\mathcal{U}}/\text{cm}^2$, (B) $\bar{g}_{Ca} = 5.5 \text{ m}\bar{\mathcal{U}}/\text{cm}^2$,
(C) $\bar{g}_{Ca} = 3.5 \text{ m}\bar{\mathcal{U}}/\text{cm}^2$, (D) $\bar{g}_{Ca} = 2.5 \text{ m}\bar{\mathcal{U}}/\text{cm}^2$,
(E) $\bar{g}_{Ca} = 2.0 \text{ m}\bar{\mathcal{U}}/\text{cm}^2$ and (F) $\bar{g}_{Ca} = 1.0 \text{ m}\bar{\mathcal{U}}/\text{cm}^2$,
with the initial conditions for V and w were set to be
($-60.899\text{mV}, 0.014873$). Other parameters were
set as in Table 2.3
- Figure 5.5 (A) Two-parameters bifurcation structure of I versus V_K , 108
while (B) is the magnification near the LP, where CP point at
 $V_K = -61.7937\text{mV}$, for equation (2.28) with different values
of V_K using AUTO software, with the initial conditions for V
and w were set to be ($-60.899\text{mV}, 0.014873$).
Other parameters were set as in Table 2.3

Figure 5.6	(A) Two-parameters bifurcation structure of I versus V_{Ca} , while (B) is the magnification near the LP, where CP point at $V_{Ca} = 134.924\text{mV}$, for equation (2.28) with different values of V_{Ca} using AUTO software, with the initial conditions for V and w were set to be $(-60.899\text{mV}, 0.014873)$. Other parameters were set as in Table 2.3	109
Figure 5.7	(A) Two-parameters bifurcation structure of I versus \bar{g}_K , while (B) is the magnification near the LP, where CP point at $\bar{g}_K = 6.1713\text{m}\bar{\text{S}}/\text{cm}^2$, for equation (2.28) with different values of \bar{g}_K using AUTO software, with the initial conditions for V and w were set to be $(-60.899\text{mV}, 0.014873)$. Other parameters were set as in Table 2.3	110
Figure 5.8	(A) Two-parameters bifurcation structure of I versus \bar{g}_{Ca} , while (B) is the magnification near the LP, where CP point at $\bar{g}_{Ca} = 4.8\text{m}\bar{\text{S}}/\text{cm}^2$, for equation (2.28) with different values of \bar{g}_{Ca} using AUTO software, with the initial conditions for V and w were set to be $(-60.899\text{mV}, 0.014873)$. Other parameters were set as in Table 2.3	111
Figure 5.9	Summary of the stability behaviours in I versus V_K for ML model, with the initial conditions are $V = -60.899\text{mV}$ and $w = 0.014873$	112
Figure 5.10	Membrane potential waveforms for stable steady state in blue region when $V_K = -70\text{mV}$ and $I = 50\mu\text{A}/\text{cm}^2$. In this case, the initial conditions are $V = -60.899\text{mV}$ and $w = 0.014873$	113
Figure 5.11	Membrane potential waveforms for bistability of a periodic solution and a steady state in pink region when $V_K = -70\text{mV}$ and $I = 65\mu\text{A}/\text{cm}^2$. In this case, the initial conditions are $V = -60.899\text{mV}$ and $w = 0.014873$	113
Figure 5.12	Membrane potential waveforms for periodic solution in red region when $V_K = -70\text{mV}$ and $I = 100\mu\text{A}/\text{cm}^2$. In this case, the initial conditions are $V = -60.899\text{mV}$ and $w = 0.014873$	114
Figure 5.13	Membrane potential waveforms for bistability of periodic solution and stable steady state in orange region when $V_K = -55\text{mV}$ and $I = 70\mu\text{A}/\text{cm}^2$. In this case, the initial conditions are $V = -60.899\text{mV}$ and $w = 0.014873$	114

Figure 5.14 Membrane potential waveforms for bistability of steady state in yellow region when $V_K = -40\text{mV}$ and $I = 35\mu\text{A}/\text{cm}^2$. In this case, the initial conditions are $V = -60.899\text{mV}$ and $w = 0.014873$. 115

LIST OF ABBREVIATIONS

AP	Action Potential
BP	Branch Point
BT	Bogdanov-Takens
CP	Cusp Point
CPC	Cups Point of Cycles
DD	Direct Field
EEG	Electroencephalographs
EP	Equilibrium Point
FHN	FitzHugh-Nagumo
GH	Generalized Hopf (Bautin)
GUI	Graphical User Interface
H	Hopf
HH	Hodgkin-Huxley
H-H	Double Hopf
IG	Initial condition Go
IL	Initial condition Last
IVP	Initial Value Problem
LC	Limit Cycle
LP	Limit Point (fold)
LPC	Limit Point of Cycles
ML	Morris-Lecar
NN	Nullcline New
O	Orbit

ODE	Ordinary Differential Equation
RK	Runge-Kutta
RP	Resting Potential
sH	Supercritical Hopf
SM	Single points Mouse
uH	Subcritical Hopf
ZH	Zero-Hopf

LIST OF SYMBOLS

A	Identity matrix
α	Probability of activation gate to be open in FHN
α_h	Voltage-dependent ion channels, rate at for sodium ions to enter via the inactivation gate
α_m	Voltage-dependent ion channels, rate at for sodium ions to enter via the activation gate
α_n	Voltage-dependent ion channels, rate at for potassium ions to enter via the activation gate
B_r	Neighbourhood
\bar{B}_r	Equilibrium neighbourhood
β_h	Voltage-dependent ion channels, rate at for sodium ions to exit via the inactivation gate
β_m	Voltage-dependent ion channels, rate at for sodium ions to exit via the activation gate
β_n	Voltage-dependent ion channels, rate at for potassium ions to exit via the activation gate
C	Map
Ca	Calcium
C_m	Membrane capacitor
E	Membrane batteries
E_{Ca}	Membrane batteries for calcium
E_K	Membrane batteries for potassium
E_l	Membrane batteries for leak
E_{Na}	Membrane batteries for sodium
E_R	Resting potential
ε	Speed of the parameter in FHN

ζ	Image of the map
F	Function of x
g_{Ca}	Calcium conductance
g_K	Potassium conductance
g_l	Leak conductance
g_{Na}	Sodium conductance
\bar{g}_{Ca}	Calcium maximal conductance
\bar{g}_K	Potassium maximal conductance
\bar{g}_l	Leak maximal conductance
\bar{g}_{Na}	Sodium maximal conductance
γ	Slope of equation in FHN
γ_p	Image of the map
h	Probability of inactivation gate of sodium channel to be open in HH
I	Applied current
I_c	Capacitive current
I_d	Dimensionless applied current
I_i	Ionic current
id	Identity map
J	Maximal interval of existence
K	Potassium
L	Inductor
l	Leak
m	Probability of activation gate of sodium channel to be open in HH

m_∞	Probability of activation gate at steady state to be open
N	Number of dimension
Na	Sodium
n	Probability of activation gate of potassium
p	Initial value
p^*	Fixed point
Q	Electrical charge
q	Initial value
R	Maximum conductance in FHN
r	Radius
\mathbb{R}	Phase plane
S	Singleton radius
s	Continuous time
T	Bigger positive number
t	Time
t_d	Dimensionless time
τ	Smallest positive number
τ_w	Rate constant for opening calcium channel
ϕ	Temperature-like time scale factor
θ	Flow map
U	Space
V	Membrane potential
V_1	Potential at which $m_\infty = 0.5$
V_2	Reciprocal of slope of voltage dependence of m_∞

V_3	Potential at which $w_\infty = 0.5$
V_4	Reciprocal of slope of voltage dependence of w_∞
V_{Ca}	Resting potential of calcium
V_d	Dimensionless membrane potential
V_K	Resting potential of potassium
V_l	Resting potential of leak
V_{Na}	Resting potential of sodium
ν	Minimum radius
W	Dimensionless recovery variable
w	Probability of activation gate of potassium channel to be open in ML
w_∞	Probability of activation gate of potassium channel at steady state to be open in ML
ω	Asymptotic parameter
X	Lyapunov function
\bar{x}	Equilibrium point
\bar{y}	Equilibrium point
z	Time limit
Ω	Negative semi-conductance
$\bar{\Omega}$	Positive semi-conductance

**KAJIAN SISTEM DINAMIKAL UNTUK MODEL HODGKIN-HUXLEY,
FITZHUGH-NAGUMO DAN MORRIS-LECAR
UNTUK MEMBRAN SARAF**

ABSTRAK

Mekanisme isyarat yang memancar dalam satu neuron telah dimodelkan dalam neurosains matematik sejak beberapa dekad yang lalu. Salah satu model neuronal matematik yang terkenal ialah model Hodgkin-Huxley (HH) yang memodelkan dinamik saluran ionik yang tertanam di sepanjang akson. Apabila nilai parameter berubah, model HH boleh menunjukkan pelbagai sifat kualitatif yang berbeza-beza. Ini bermakna sistem saraf telah mengalami perubahan dan ini mungkin berhubung kait dengan penyakit neuron tertentu. Diagnosis perubatan yang baharu boleh dibuat dengan membawa kembali nilai-nilai parameter ke julat yang munasabah. Oleh itu, adalah sangat penting untuk menganalisis sistem dinamik satu model neuron tunggal dalam rajah bifurkasi satu dan dua parameter, dan mengkaji kestabilan setiap rantau parameter dengan menggunakan simulasi komputer XPPAut dan MatCont. Memandangkan sebuah model HH terdiri daripada empat persamaan pembezaan, para saintis telah menurunkan model HH kepada dua persamaan pembezaan untuk mengurangkan beban pengkomputeran dalam kajian neuronal yang lebih kompleks. Model yang diringkaskan seperti model FitzHugh-Nagumo (FHN) dan model Morris-Lecar (ML) sepatutnya dapat menjelaskan pandangan dinamik mekanisma satu neuron tunggal dengan cara yang lebih ringkas atau lebih mudah tanpa kehilangan apa-apa sifat dinamik daripada pemodelan asal. Malangnya, dalam proses penurunan, beberapa pemboleh ubah perlu dihapuskan dan mengakibatkan beberapa pautan kualitatif kepada data biologi turut hilang. Dengan membandingkan

keputusan dalam rajah bifurkasi satu dan dua parameter, kesimpulan dapat dibuat bahawa FHN ialah satu model kualitatif yang hanya menghasilkan semula ciri-ciri utama pola dinamik neuronal satu potensi tindakan (AP), tanpa membekalkan maklumat biologi yang dapat diukur. Bentuk gelombang letusan yang diperhatikan dalam model ML boleh membawa lebih banyak kandungan maklumat berbanding bentuk gelombang berkala yang stabil. Namun demikian, neuron yang tidak meletus secara terpencil boleh menghasilkan aktiviti letusan dalam satu rangkaian. Model HH mempunyai rantau letusan dalam struktur global. Oleh itu, walaupun rantau tersebut berada dalam skala arus suntikan negatif, model HH tetap berpotensi menghasilkan gelombang letusan jika nilai parameter diubah sehingga dapat membawa rantau letusan tersebut ke dalam skala arus suntikan positif disebabkan AP hanya boleh menghasilkan tindakbalas dalam skala arus suntikan positif.

**DYNAMICAL SYSTEM STUDY OF THE HODGKIN-HUXLEY,
FITZHUGH-NAGUMO AND MORRIS-LECAR MODELS
OF NERVE MEMBRANES**

ABSTRACT

The mechanism of signals transmitting in a single neuron has been modelled in mathematical neuroscience since the past few decades. One of the well-known mathematical neuronal models is the Hodgkin-Huxley (HH) model that models the dynamics of ionic channels embedded along the axon. When parameter values are varied, the HH model can show a variety of different qualitative behaviours. This means that the nervous system has been altered and this might relate to some neuronal diseases. New medical diagnosis can be made by bringing the parameter values back to its reasonable range. Thus, it is very important to analyse the dynamical systems of a single neuron model in one- and two-parameters bifurcation diagrams, and to study the stabilities of each parameter regions using computer simulations XPPAut and MatCont. Since a HH model consists of 4-differential equations, scientists have reduced the HH model to two-parameters differential equations to reduce the computational load of a more complex neuronal study. Reduced models such as the FitzHugh-Nagumo (FHN) and Morris-Lecar (ML) models are supposed to be able to explain the dynamical view of the mechanism of a single neuron in a better or simpler way without losing any dynamical properties from the original modelling. Unfortunately, in the reducing process, some variables need to be eliminated and this means that some qualitative links to biological data are lost. By comparing the results in one- and two-parameter bifurcation diagrams, we can conclude that FHN is a qualitative model that only reproduces the main features

of neuronal dynamics patterns of action potential (AP), without providing quantifiable biological information. Bursting waveforms that we observed in ML model can carry more informational content compared to stable periodic waveforms. Even so, neurons that do not burst in isolation can often produce bursting activity in a network. HH already has bursting region in a global structure. Therefore, despite being in negative scale of injection current, the possibility for HH to spike a series of bursting AP still exists, if we vary the parameter so that the bursting region is moved into a positive scale of injection current since AP can only be activated in positive scale of injection current.

CHAPTER 1

INTRODUCTION

1.1 Preliminary

The predominant question is how does the brain process information? For instance, if a human touches a hot stove with his hand, the sensory organs from his hand send information to the brain, which consequently registers the data and returns a message to the hand to pull away. To understand the mechanism of information processing and impulse transmission in the brain, it is important to understand the dynamical system of single neuron in neuronal model.

The first chapter introduces the mechanism of single neuron and the mechanism of signal transmission. To further clarify the principal facts of the thesis, the main terminologies such as resting potential (RP) and action potential (AP) will be defined first. RP refers to the electrical potential along the membrane when the nerve cells are not stimulated by impulses while AP refers to short-lasting event of electrical potential which contain impulses along the membrane of the nerve cells (Hodgkin and Huxley, 1952a; 1952b; 1952c; 1952d; Hodgkin et al., 1952). This chapter also discuss the theoretical and concept of dynamical system applied on nerve membrane models in this whole thesis.

Subsequently, the next section elaborates the motivation, problem statements, objectives, and significance of the research. The last section presents an overview of the outline and organization of the thesis.

1.2 Mechanism of Single Neuron

Neurons exist in many different shapes and sizes but share certain characteristics (Kandel et al., 2000; Bear et al., 2007). Figure 1.1 shows a schematic view of a neuron. The neuron structure can be divided into three basic parts, namely soma, axon and dendrites. The soma plays a key role in the actual processing of information that passes through the neuron. The axon acts like an ‘output cable’ of a neuron and the length can reach 1 meter in humans. The axon shape is thin and similar to the cell cable-like projections which convey electrochemical messages in the form of an electric signal or APs. Information from soma travels down the axon allowing the neuron to communicate with other neurons or other cells. The third part of the neuron is dendrite, an extension of the neuron cell body, and it specializes in receiving and processing excitatory synaptic inputs from other neurons.

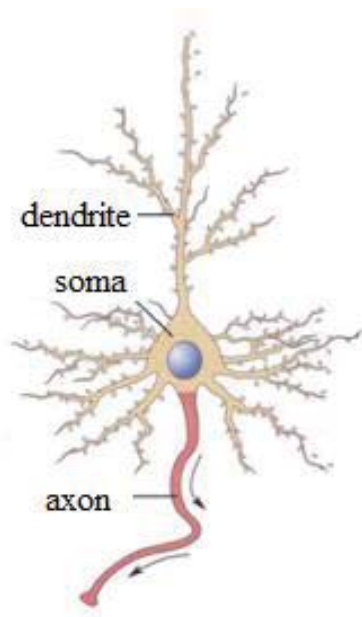


Figure 1.1: The general structure of a neuron (Bear et al., 2007)

Neuron's cell membrane is made of a lipid bilayer which comprises protein ionic channels, thus preventing ions from flowing freely through it (Marbán, 2002). The cells have various mechanisms of transportation that allow different types of ions to cross the plasma membrane via its ionic channels embedded along the neuron with their own corresponding characteristics, resulting in a net imbalance of charges or concentration gradients. Figure 1.2 shows major ionic constituents, namely sodium ions Na^+ , potassium ions K^+ and calcium ions Ca^{2+} residing in a single neuron. These ions diffuse their electrochemical gradient via dependent voltage or dependent ligand gated channels. These ion channels render the cell membrane selectively permeable to various ions and other substances (like glucose). The selective permeability of the cell membrane allows the inner part to have a different composition from the outer part of the membrane. This creates a potential difference across the membrane along the long cylindrical membrane.

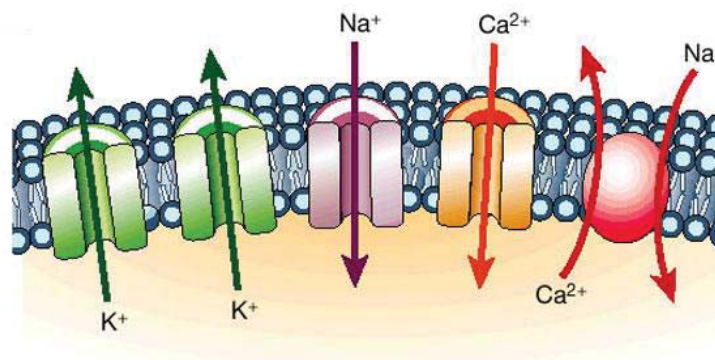


Figure 1.2: Ion channels function as pores to permit the flux of ions down their electrochemical potential gradient (Marbán, 2002)

1.2.1 Resting Potential

A disturbance such as mechanical, electrical, or sometimes chemical disruption triggers a few sodium channels in a small portion of the membrane to open causing sodium ions to flow into the cell and potassium ions to flow out (Bear et al., 2007). The positive charge from the sodium ions produces less negativity inside the cell (depolarizes the cell), thus their RP is at -60 mV to -80 mV (Lodish et al., 2000). If the RP is increased above a certain threshold value, more sodium channels in that area will open. More sodium that flows in can trigger an AP. The inflow of sodium ions reverses the membrane potential in that area, making it positive inside the cell and negative outside the cell. These processes have the net effect of locally increasing the potential within the neuron to about $+40$ mV before it is restored to the RP, where potassium ions leave the cell through the open potassium channels rendering it more negative inside the cell (see Figure 1.3). The whole process lasts for about 1 ms. The membrane potential slightly overshoots the resting potential, which is corrected by the sodium-potassium pump, and restores the normal ion balance across the membrane, subsequently returning the membrane potential to its resting level. This results in a voltage difference or AP which prompts the nerve pulse to provide the key method in transmitting information (Bear et al., 2007).

1.2.2 Action Potential

AP refers to a series of sudden changes in the electric potential as ions flow across the plasma membrane of a neuron. The process is repeated and finally, the signal courses down the entire length of the neuron. Then, an electrical charge or a release of neurotransmitters such as serotonin or dopamine allows the signal to leap across a

gap called a synapse to the next neuron. Neurons do not fire on their own; they fire as a result of incoming spikes from other neurons.

Circuits of neurons in the brain are complicated due to the multiple nonlinearities, different types of neurons, complex dendritic geometries, diverse connectivity patterns and dependencies on learning and development. Neurologists use electroencephalographs (EEGs) to record the overall electrical activity in the brain via electrodes placed on the scalp.

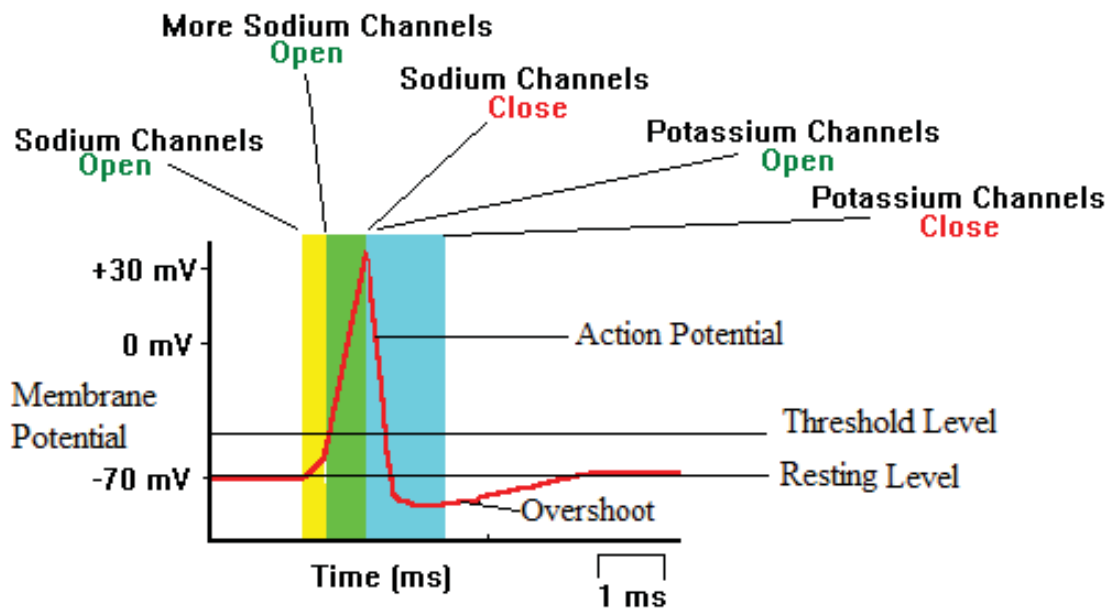


Figure 1.3: Recording of an AP in an axon following stimulation due to changes in the permeability of the cell membrane to sodium and potassium ions (Lodish et al., 2000)

1.3 Theoretical and Concept of Dynamical Systems

1.3.1 Dynamical Systems

Definition 1.1: Dynamical systems. Dynamical systems refers to the system in which a function describes the time dependence of a point in a geometrical space. The evolution rule of dynamical systems is an implicit relation of differential equations that gives the state of the system for only a short time into the future. If the system can be solved by given an initial condition, it is possible to determine all its future positions and collection of points known as a trajectory or orbit (Blanchard et al., 2006).

Let U be an open subset in \mathbb{R}^N on a C^1 map

$$\theta: \mathbb{R} \times U \rightarrow U, \quad (1.0)$$

which satisfies the group action axioms:

$$\theta(0, p) = p, \quad \text{for all } p \in U, \quad (1.1)$$

and

$$\theta(t+s, p) = \theta(t, \theta(s, p)), \quad \text{for all } p \in U, \text{ and all } t, s \in \mathbb{R}. \quad (1.2)$$

Thus, a continuous dynamical system can be thought of as a C^1 action of the group $(\mathbb{R}, +)$ on the open set $U \subseteq \mathbb{R}^N$ (Adolfo, 2019).

Example 1.1. Let $F: U \rightarrow \mathbb{R}^N$ be a C^1 vector field. Then, the flow map, θ , of F defined as a dynamical system if, for all $p \in U$, the initial value problem (IVP)

$$\frac{dx}{dt} = F(x), \quad (1.3)$$

with initial

$$x(0) = p, \quad (1.4)$$

has a solution that exist for all $t \in \mathbb{R}$ (Adolfo, 2019).

Example 1.2. Define $\theta: \mathbb{R} \times \mathbb{R}^2 \rightarrow \mathbb{R}^2$ by

$$\theta\left(t, \begin{pmatrix} p \\ q \end{pmatrix}\right) = \begin{pmatrix} \cos t & -\sin t \\ \sin t & \cos t \end{pmatrix} \begin{pmatrix} p \\ q \end{pmatrix}, \text{ for } t, p, q \in \mathbb{R}. \quad (1.5)$$

To see that θ defines a dynamical system, first observe that

$$\theta\left(0, \begin{pmatrix} p \\ q \end{pmatrix}\right) = A \begin{pmatrix} p \\ q \end{pmatrix}, \quad (1.6)$$

where A denotes that 2x2 identity matrix. Consequently,

$$\theta\left(0, \begin{pmatrix} p \\ q \end{pmatrix}\right) = \begin{pmatrix} p \\ q \end{pmatrix}. \quad (1.7)$$

Finally, we use the trigonometric identities

$$\begin{aligned} \cos(t+s) &= \cos t \cos s - \sin t \sin s \\ \sin(t+s) &= \cos t \sin s + \sin t \cos s \end{aligned} \quad (1.8)$$

to verify that

$$\theta\left(t, \begin{pmatrix} p \\ q \end{pmatrix}\right) = \begin{pmatrix} \cos t & -\sin t \\ \sin t & \cos t \end{pmatrix} \begin{pmatrix} \cos s & -\sin s \\ \sin s & \cos s \end{pmatrix} \begin{pmatrix} p \\ q \end{pmatrix}, \quad (1.9)$$

from which we obtain that

$$\theta\left(t+s, \begin{pmatrix} p \\ q \end{pmatrix}\right) = \theta\left(t, \theta\left(s, \begin{pmatrix} p \\ q \end{pmatrix}\right)\right). \quad (1.10)$$

For each $t \in \mathbb{R}$, the dynamical system, $\theta: \mathbb{R} \times U \rightarrow U$, induces a map on U , denoted by $\theta_t: U \rightarrow U$, and given by

$$\theta_t(p) = \theta(t, p), \quad \text{for all } p \in U. \quad (1.11)$$

The map $\theta_t: U \rightarrow U$ defined by (1.10) is C^1 . Furthermore, it follows from (1.1) and (1.2) that

$$\theta_t \cdot \theta_{-t} = id, \quad (1.12)$$

where id denoted the identity map in U , and

$$\theta_{-t} \cdot \theta_t = id. \quad (1.13)$$

It then follows that θ_t is invertible with inverse θ_{-t} . Hence, θ_t is C^1 with an inverse which is also C^1 . We say that θ_t is a diffeomorphism of U . Hence, a dynamical system θ_t induces a family of diffeomorphisms, $\{\theta_t\}_{t \in \mathbb{R}}$, of the set U into itself (Adolfo, 2019).

1.3.2 Orbits

Definition 1.2: Orbits. Let $\theta(t, p)$ denote a dynamical system on an open set $U \subseteq \mathbb{R}^N$ (Adolfo, 2019). Given $p \in U$, the orbit of the flow, θ_t , through p is the set, ζ_p , defined by

$$\zeta_p = \{x \in U \mid x = \theta(t, p) \text{ for some } t \in \mathbb{R}\}, \quad (1.14)$$

or in other words, ζ_p is the image of the map $\theta_p : \mathbb{R} \rightarrow U$ defined by

$$\theta_p(t) = \theta(t, p), \quad \text{for all } t \in \mathbb{R}. \quad (1.15)$$

Example 1.3. For the dynamical system $\theta : \mathbb{R} \times \mathbb{R}^2 \rightarrow \mathbb{R}^2$ as in Example 1.2, $\zeta_{(p,q)}$ is

a circle of radius $\sqrt{p^2 + q^2}$ around the origin for the case $(p, q) \neq (0, 0)$; and

$\zeta_{(0,0)} = \{(0, 0)\}$. Figure 1.4 shows $\zeta_{(1,0)}$, $\zeta_{(0,0)}$ and another typical orbit of the

dynamical system θ (Adolfo, 2019). The arrows on the two circular orbits portrayed

in the figure indicate the direction on the orbit induced by the parameterization

$\theta_{(p,q)} : \mathbb{R} \rightarrow \mathbb{R}^2$ defined by

$$\theta_{(p,q)}(t) = \theta\left(t, \begin{pmatrix} p \\ q \end{pmatrix}\right), \text{ for all } t \in \mathbb{R}, \quad (1.16)$$

at t increases.

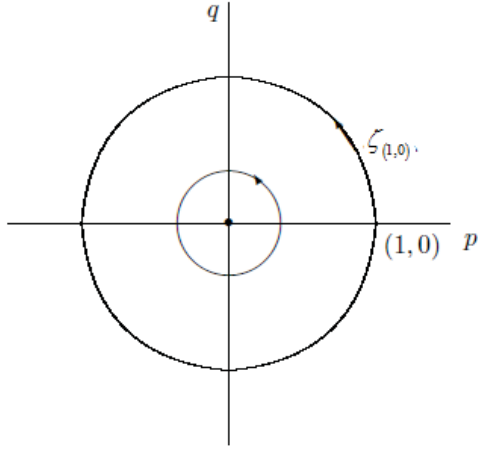


Figure 1.4: Phase portrait of θ in Example 1.2 (Adolfo, 2019)

1.3.3 Phase Portrait

Definition 1.3: Phase portrait. A depiction of all possible kinds of orbits that a dynamical system can have is known as a phase portrait of the systems (Adolfo, 2019).

Example 1.4. Figure 1.4 shows the phase portrait of the dynamical systems, $\theta: \mathbb{R} \times \mathbb{R}^2 \rightarrow \mathbb{R}^2$ as in Example 1.2. Observe that, for $(p, q) \neq (0, 0)$ and $\theta_{(p,q)}$ as defined in (1.16),

$$\begin{aligned}
 \|\theta_{(p,q)}(t)\|^2 &= (p \cos t - q \sin t)^2 + (p \sin t + q \cos t)^2 \\
 &= p^2 \cos^2 t - 2pq \sin t \cos t + q^2 \sin^2 t \\
 &\quad + p^2 \sin^2 t + 2pq \sin t \cos t + q^2 \cos^2 t \\
 &= p^2 + q^2, \quad \text{for all } t \in \mathbb{R},
 \end{aligned} \tag{1.17}$$

which shows that $\zeta_{(p,q)}$ lies in the circle of radius $r = \sqrt{p^2 + q^2}$ around the origin in \mathbb{R}^2 . On the other hand, if $(x, y) \in S_r \setminus \{(0, 0)\}$, the circle of the radius r around the origin in \mathbb{R}^2 , where $r > 0$, by letting

$$t = \arctan\left(\frac{y}{x}\right) - \arctan\left(\frac{q}{p}\right), \quad (1.18)$$

we can show that

$$\theta_{(p,q)}(t) = \begin{pmatrix} x \\ y \end{pmatrix}. \quad (1.19)$$

In other words, $(x, y) \in \zeta_{(p,q)}$. Consequently, $\zeta_{(p,q)} = S_r((0,0))$, for $r = \sqrt{p^2 + q^2}$, as claimed in Example 1.3. On the other hand, if $(p, q) = (0,0)$, then $\zeta_{(p,q)} = \{(0,0)\}$.

Thus, the singleton $\{(0,0)\}$ and concentric circle around the origin are the only kinds of orbits that the dynamical system, $\theta(t, p)$, defined in Example 1.3 can have (Adolfo, 2019).

1.3.4 Infinitesimal Generator

Given a dynamical system, $\theta: \mathbb{R} \times U \rightarrow U$, on an open set $U \subseteq \mathbb{R}^N$, we can define a vector field, $F: U \rightarrow \mathbb{R}^N$ (Adolfo, 2019), as follows:

$$F(x) = \frac{\partial}{\partial t} \theta(t, x) \Big|_{t=0} \quad \text{for all } x \in U, \quad (1.20)$$

or in other words,

$$F(x) = \lim_{z \rightarrow 0} \frac{\theta(z, x) - \theta(0, x)}{z}, \quad \text{for all } x \in U. \quad (1.21)$$

Since we are assuming that the dynamical system, $\theta: \mathbb{R} \times U \rightarrow U$ is a C^1 map, it follows that $F: U \rightarrow \mathbb{R}^N$ defined in (1.20) is a C^1 vector field defined in U . We show next that $\theta: \mathbb{R} \times U \rightarrow U$ is the flow map for the vector field F . The vector field, F , defined in (1.21) is called the infinitesimal generator of the dynamical system θ_t , for $t \in \mathbb{R}$ (Adolfo, 2019).

Thus, we need to show that the map $\theta_p : \mathbb{R} \rightarrow U$, given by

$$\theta_p(t) = \theta(t, p), \quad \text{for all } t \in \mathbb{R} \quad (1.22)$$

is the unique solution to the IVP in (1.3).

Using the group action axiom for $\theta(t, p)$ in (1.2), we see that θ_p defined in (1.22) satisfies

$$\theta_p(t+z) = \theta(t+z, p) = \theta(z, \theta(t, p)), \text{ for } t, z \in \mathbb{R}. \quad (1.23)$$

We then have that

$$\theta_p(t+z) = \theta(z, \theta_p(t)), \quad \text{for } t, z \in \mathbb{R}. \quad (1.24)$$

Thus, for $z \neq 0$ we obtain from (1.24) that

$$\frac{\theta_p(t+z) - \theta_p(t)}{z} = \frac{\theta(z, \theta_p(t)) - \theta(0, \theta_p(t))}{z}, \quad (1.25)$$

where we have also used the group action axiom for $\theta(t, p)$ in (1.1) (Adolfo, 2019).

Next, letting $z \rightarrow 0$ in (1.25) and using the definition of the field, F , in (1.21), we obtain that

$$\theta_p'(t) = F(\theta_p(t)), \quad (1.26)$$

where prime (') denote the differentiation with respect to t . Equation (1.26) shows that θ_p solves the differential equation in the IVP (1.3). Finally, since $\theta_p(0) = p$, by the group action axiom for $\theta(t, p)$ in (1.1), we see that $\theta_p : \mathbb{R} \rightarrow U$ solves the IVP in (1.3), which was to be shown.

Example 1.5. Let $\theta : \mathbb{R} \times \mathbb{R}^2 \rightarrow \mathbb{R}^2$ be the dynamical system given in Example 1.2 (Adolfo, 2019). To find the infinitesimal generator of θ , we first compute

$$\frac{\partial \theta}{\partial t} \left(t, \begin{pmatrix} x \\ y \end{pmatrix} \right) = \begin{pmatrix} -\sin t & -\cos t \\ \cos t & -\sin t \end{pmatrix} \begin{pmatrix} x \\ y \end{pmatrix}, \text{ for all } \begin{pmatrix} x \\ y \end{pmatrix} \in \mathbb{R}^2, \quad (1.27)$$

so that

$$\begin{aligned}
 F\begin{pmatrix} x \\ y \end{pmatrix} &= \frac{\partial \theta}{\partial t}\left(0, \begin{pmatrix} x \\ y \end{pmatrix}\right) \\
 &= \begin{pmatrix} 0 & -1 \\ 1 & 0 \end{pmatrix} \begin{pmatrix} x \\ y \end{pmatrix} \\
 &= \begin{pmatrix} -y \\ x \end{pmatrix},
 \end{aligned} \tag{1.28}$$

for all $\begin{pmatrix} x \\ y \end{pmatrix} \in \mathbb{R}^2$. It then follows that the infinitesimal generator of θ is the vector

field, $F: \mathbb{R}^2 \rightarrow \mathbb{R}^2$, given by

$$F\begin{pmatrix} x \\ y \end{pmatrix} = \begin{pmatrix} -y \\ x \end{pmatrix}, \quad \text{for all } \begin{pmatrix} x \\ y \end{pmatrix} \in \mathbb{R}^2. \tag{1.29}$$

In other words, the dynamical system, $\theta: \mathbb{R} \times \mathbb{R}^2$, given by

$$\theta\left(t, \begin{pmatrix} p \\ q \end{pmatrix}\right) = \begin{pmatrix} \cos t & -\sin t \\ \sin t & \cos t \end{pmatrix} \begin{pmatrix} p \\ q \end{pmatrix}, \quad \text{for } t, p, q \in \mathbb{R}, \tag{1.30}$$

is the flow of the linear system of differential equations

$$\frac{dx}{dt} = -y, \tag{1.31}$$

and

$$\frac{dy}{dt} = x. \tag{1.32}$$

1.3.5 Fixed Points and Equilibrium Solutions

Attractive fixed points are a special case of a wider mathematical concept of attractors where this point occurs when there is an intersection of trajectories. An attractive fixed point is said to be a stable fixed point if it is also a Lyapunov stable and this Lyapunov stable leads to periodic orbit (Lyapunov, 1966).

Let $\theta: \mathbb{R} \times U \rightarrow U$ be a C^1 dynamical system in U with infinitesimal generator $F: U \rightarrow \mathbb{R}^N$ (Adolfo, 2019). A fixed point of the flow θ_t in U is a point $p^* \in U$ such that

$$\theta(t, p^*) = p^*, \quad \text{for all } t \in \mathbb{R}, \quad (1.33)$$

or

$$\theta_{p^*}(t) = p^*, \quad \text{for all } t \in \mathbb{R}. \quad (1.34)$$

Taking the derivative with respect to t on both sides of (1.34) we obtain that

$$\theta'_{p^*}(t) = 0, \quad \text{for all } t \in \mathbb{R}, \quad (1.35)$$

so that, by the definition of the infinitesimal generator of θ_t ,

$$F(\theta_{p^*}(t)) = 0, \quad \text{for all } t \in \mathbb{R}. \quad (1.36)$$

Combining (1.34) with (1.36) we obtain

$$F(p^*) = 0. \quad (1.37)$$

Thus, a fixed point of the dynamical system with infinitesimal generator $F: U \rightarrow \mathbb{R}^N$ is a solution to the equation

$$F(p) = 0. \quad (1.38)$$

Solutions to (1.38) are also known as equilibrium points, or singular points. A point $p \in U$ which is not a fixed point of the system generated by F is called a regular point of F . A solution to the system (1.3) defined by (1.34) where $p^* \in U$ satisfies (1.37) is called an equilibrium solution (Adolfo, 2019).

Example 1.6. Consider the two-dimensional system

$$\frac{dx}{dt} = \lambda x + y, \quad (1.39)$$

and

$$\frac{dy}{dt} = \lambda y. \quad (1.40)$$

where $\lambda \neq 0$.

In this case the field, $F : \mathbb{R}^2 \rightarrow \mathbb{R}^2$, is given by

$$F \begin{pmatrix} x \\ y \end{pmatrix} = \begin{pmatrix} \lambda x + y \\ \lambda x \end{pmatrix}, \quad \text{for all } \begin{pmatrix} x \\ y \end{pmatrix} \in \mathbb{R}^2. \quad (1.41)$$

The equilibrium points are therefore solutions to the system

$$\lambda x + y = 0, \quad (1.42)$$

and

$$\lambda y = 0. \quad (1.43)$$

Since $\lambda \neq 0$, the only solution to the system in (1.42) and (1.43) is the origin, $(0,0)$, in \mathbb{R}^2 . Thus, $(0,0)$ is the only equilibrium point of the system in (1.39) and (1.40) (Adolfo, 2019).

1.3.6 Cycles and Periodic Solutions

A periodic solution is a function that repeated values in regular intervals or periods. Periodic solutions are used to describe oscillations of waves. The appearance or the disappearance of a periodic solution through a local change in the stability properties of a steady point is known as Hopf bifurcation in codimension of bifurcation (Blanchard et al., 2006).

Definition 1.4: Cycles. An orbit of a dynamical system is called a cycle when it is a simple closed curve (Adolfo, 2019).

Let $\theta : \mathbb{R} \times U \rightarrow U$ be a dynamical system in an open set $U \subseteq \mathbb{R}^N$. Suppose that for $p \in U$, the orbit of p , ζ_p , is a cycle. Then, there exists a positive number T such

that $\theta_p(T, p) = p$ and $\theta_p : [0, T] \rightarrow U$ is a parameterization of ζ_p . In other words, $\theta_p : [0, T] \rightarrow U$ is one-to-one, and $\zeta_p = \theta_p([0, T])$. The function θ_p is said to be periodic with period T .

Definition 1.5: Periodic solutions. Let $U \subseteq \mathbb{R}^N$ be open and $F : U \rightarrow \mathbb{R}^N$ be a C^1 vector field. A solution $u : \mathbb{R} \rightarrow U$ of differential equation in (1.3) which is not an equilibrium solution, is said to be periodic if there exists a positive number, τ , such that

$$u(t + \tau) = u(t), \quad \text{for all } t \in \mathbb{R}. \quad (1.44)$$

The smallest positive number, τ , for which (1.44) is called the period of u (Adolfo, 2019).

Example 1.7. Suppose that the differential equation in (1.3) has a flow, $\theta : \mathbb{R} \times U \rightarrow U$, and that the orbit, ζ_p , for $p \in U$, is a cycle. Let $T > 0$ be such that

$$\theta(T, p) = p, \quad (1.45)$$

$$\theta_p([0, T]) = \zeta_p, \quad (1.46)$$

and

$$\theta_p : [0, T] \rightarrow U \text{ is one-to-one.} \quad (1.47)$$

We show that the function

$$\theta_p : \mathbb{R} \rightarrow U \quad (1.48)$$

is periodic with period T . To see why this claim is true, observe that, for any $t \in \mathbb{R}$,

$$\theta(t + T, p) = \theta(t, \theta(T, p)) = \theta(t, p), \quad (1.49)$$

where we have used (1.45). We therefore have that

$$\theta_p(t + T) = \theta_p(t), \quad \text{for all } t \in \mathbb{R}, \quad (1.50)$$

which shows that θ_p is periodic (Adolfo, 2019).

1.3.7 Lyapunov Stability

Various types of stability may be discussed for the solutions of differential equations in describing dynamical systems especially the stability of solutions near to the equilibrium point. If all solution nears the attractive fixed point converge to equilibrium point, it known as Lyapunov stable or also known as asymptotically stable (Lyapunov, 1966).

Let U denote an open subset of \mathbb{R}^N and $F:U \rightarrow \mathbb{R}^N$ be a C^1 vector field. Suppose that \bar{x} is an equilibrium point of the system in (1.3). Assume also that there exists $\bar{r} > 0$ such that $\bar{B}_{\bar{r}}(\bar{x}) \subset U$, and $\bar{B}_{\bar{r}}(\bar{x}) \setminus \{\bar{x}\}$ contains no equilibrium points of F ; in other words, \bar{x} is an isolated equilibrium point of F in U . In this section we are interested in conditions that will guarantee that if a solution of (1.3) begins near the equilibrium point, \bar{x} , then it will remain near \bar{x} for all $t > 0$. This is the concept of stability which we make precise in the following definition (Adolfo, 2019).

Definition 1.6: Lyapunov stability. Let \bar{x} be an isolated equilibrium point of the system in (1.3) and let $\bar{r} > 0$ be such that $\bar{B}_{\bar{r}}(\bar{x}) \subset U$, and $\bar{B}_{\bar{r}}(\bar{x}) \setminus \{\bar{x}\}$ contains no equilibrium points on F (Adolfo, 2019). We say that \bar{x} is stable if, for every $r \in (0, \bar{r})$, there exists $\delta > 0$ such that, if $\|p - \bar{x}\| < \delta$, then the solution, $u_p : J_p \rightarrow U$, to the IVP (1.3) exists for all $t > 0$, and there exists $t_1 > 0$ such that

$$u_p(t) \in \bar{B}_r(\bar{x}), \quad \text{for } t \geq t_1, \quad (1.51)$$

where J_p is the maximal interval of existance.

Definition 1.7: Asymptotic stability. An isolated equilibrium point, \bar{x} , of the system in (1.3) is said to be asymptotically stable if \bar{x} is stable and there exists $\delta > 0$ such that, if $\|p - \bar{x}\| < \delta$, then $\omega(\zeta_p) = \{\bar{x}\}$ (Adolfo, 2019).

Definition 1.8: Unstable equilibrium points. An isolated equilibrium point, \bar{x} , of the system in (1.3) which is not stable is said to be unstable (Adolfo, 2019).

Example 1.8. Consider the system

$$\frac{dx}{dt} = y + \mu x^3 \quad (1.52)$$

and

$$\frac{dy}{dt} = -x + \mu y^3, \quad (1.53)$$

where $\mu > 0$. We want to show that $(0, 0)$ is an unstable equilibrium point of the system in (1.52) and (1.53) (Adolfo, 2019). First, note that $(0, 0)$ is the only equilibrium point of the system in (1.52) and (1.53). Indeed, suppose that (\bar{x}, \bar{y}) is an equilibrium point of the system in (1.52) and (1.53) with $(\bar{x}, \bar{y}) \neq (0, 0)$. We then have that

$$\bar{y} + \mu \bar{x}^3 = 0 \quad (1.54)$$

and

$$-\bar{x} + \mu \bar{y}^3 = 0. \quad (1.55)$$

We see that $\bar{x} \neq 0$ and $\bar{y} \neq 0$. To show the impossible case for \bar{x} and \bar{y} , suppose that $\bar{x} = 0$ in (1.55), we get $\bar{y} = 0$ since $\mu > 0$, which is impossible since we are assuming that $(\bar{x}, \bar{y}) \neq (0, 0)$. Similarly, $\bar{y} = 0$. Next, multiply (1.54) by \bar{x} and (1.55) by \bar{y} to get

$$\bar{x}\bar{y} + \mu \bar{x}^4 = 0 \quad (1.56)$$

and

$$-\bar{x}\bar{y} + \mu \bar{y}^4 = 0. \quad (1.57)$$

Adding (1.56) and (1.57) we get

$$\mu(\bar{x}^4 + \bar{y}^4) = 0, \quad (1.58)$$

which yields that

$$\bar{x}^4 + \bar{y}^4 = 0, \quad (1.59)$$

since $\mu > 0$. Note that (1.59) is impossible for $(\bar{x}, \bar{y}) \neq (0, 0)$. We have therefore

shown that $(0, 0)$ is an isolated equilibrium point of the system in (1.52) and (1.53).

Next, we show that $\mu > 0$ implies that $(0, 0)$ is unstable by letting $(p, q) \neq (0, 0)$ be

such that $p^2 + q^2 < \delta$ and let $u_{(p,q)} : J_{(p,q)} \rightarrow \mathbb{R}^2$ denote the solution to the system in

(1.52) and (1.53) subject to initial condition

$$(x(0), y(0)) = (p, q). \quad (1.60)$$

Suppose by way of contradiction that

$$u_{(p,q)}(t) \in \bar{B}_r(0, 0), \quad \text{for all } t \in J_{(p,q)} \cap [0, +\infty). \quad (1.61)$$

It follows from (1.61) that $u_{(p,q)}$ is defined for all $t \geq 0$.

Let's define $X(x, y) = x^2 + y^2$ for all $(x, y) \in \mathbb{R}^2$ and put

$$u_{(p,q)}(t) = (x(t), y(t)), \quad \text{for all } t \geq 0. \quad (1.62)$$

Applying the Chain Rule we obtain that

$$\frac{d}{dt} [X(u_{(p,q)}(t))] = 2\mu [(x(t))^4 + (y(t))^4], \quad \text{for all } t \geq 0. \quad (1.63)$$

Note also that, since $(p, q) \neq (0, 0)$, it follows from uniqueness that

$$u_{(p,q)}(t) \neq (0, 0), \quad \text{for all } t \geq 0 \quad (1.64)$$

thus, (1.63) become

$$\frac{d}{dt} [X(u_{(p,q)}(t))] > 0, \quad \text{for all } t \geq 0, \quad (1.65)$$

since $\mu > 0$. Consequently, $X(u_{(p,q)}(t))$ is increasing in t . Thus,

$$X(u_{(p,q)}(t)) \geq X(p,q), \quad \text{for all } t \geq 0. \quad (1.66)$$

Using the definition of X and (1.61), we obtain from (1.66) that

$$r_0 \leq \|u_{(p,q)}(t)\| \leq r, \quad \text{for all } t \geq 0, \quad (1.67)$$

where $r_0 = \|(p,q)\|$. Since we are assuming that $(p,q) \neq (0,0)$, we have that $r_0 > 0$.

Put

$$v = \min_{r_0 \leq \|(x,y)\| \leq r} 2\mu(x^4 + y^4). \quad (1.68)$$

Then, $v > 0$ since $r_0 > 0$ and $x^4 + y^4 = 0$ if and only if $(x,y) = (0,0)$. It follows

from (1.63), (1.67) and (1.68) that

$$\frac{d}{dt} [X(u_{(p,q)}(t))] \geq v \quad \text{for all } t \geq 0. \quad (1.69)$$

Integrating the inequality in (1.69) from 0 to t then yields

$$X(u_{(p,q)}(t)) \geq X(p,q) + vt, \quad \text{for all } t \geq 0, \quad (1.70)$$

which implies that

$$\|u_{(p,q)}(t)\| \rightarrow \infty \quad \text{as } t \rightarrow \infty, \quad (1.71)$$

which contradicts (1.61). This contradiction shows that $(0,0)$ is an unstable equilibrium point for the system in (1.52) and (1.53) for $\mu > 0$ (Adolfo, 2019).

Definition 1.9: Lie derivation. Let $F:U \rightarrow \mathbb{R}^N$ be a C^1 vector field on a open subset, U , of \mathbb{R}^N (Adolfo, 2019). Given a C^1 function, $X:U \rightarrow \mathbb{R}$, we define the derivative of X along orbits of the system in (1.3) to be map $\dot{X}:U \rightarrow \mathbb{R}$ given by

$$\dot{X}(x) = \nabla X \cdot F(x), \quad \text{for all } x \in U \quad (1.72)$$

where ∇ denotes the gradient of X .

Definition 1.10: Lyapunov function. Let U be an open subset of \mathbb{R}^N and Ω be an open subset of U with $\bar{\Omega} \subset U$ (Adolfo, 2019). A C^1 function, $X : U \rightarrow \mathbb{R}$, is said to be a Lyapunov function of the system in (1.3) in on the set Ω if and only if

$$\dot{X}(x) \leq 0, \quad \text{for all } x \in \Omega. \quad (1.73)$$

Definition 1.11: Positive definite functions. Let $\Omega \subset \bar{\Omega} \subset U$ be a neighbourhood of 0. Let $X : U \rightarrow \mathbb{R}$ be a continuous function satisfying $X(0) = 0$. We say that X is positive semi-definite in $\bar{\Omega}$ if $X(x) \geq 0$ for all $x \in \bar{\Omega}$. We say that X is positive definite in $\bar{\Omega}$ if $X(x) > 0$ for all $x \in \bar{\Omega} \setminus \{0\}$ and $X(0) = 0$ (Adolfo, 2019).

Definition 1.12: Negative definite functions. Let $\Omega \subset \bar{\Omega} \subset U$ be a neighbourhood of 0. Let $X : U \rightarrow \mathbb{R}$ be a continuous function satisfying $X(0) = 0$. We say that X is negative semi-definite in Ω if $-X$ is positive semi-definite. We say that X is negative definite in Ω if $-X$ positive definite (Adolfo, 2019).

Theorem 1.1: Lyapunov Stability Theorem. Let $\bar{x} = \{0\}$ be an isolated equilibrium point of the system in (1.3). Suppose that the system in (1.3) has Lyapunov function, X , in a neighbourhood $\Omega \subset \bar{\Omega} \subset U$ of 0. Assume also that X is positive definite in Ω . Then $\bar{x} = 0$ is a stable equilibrium point of the system in (1.3). In addition, if V is negative definite in Ω , then $\omega(\gamma_p) = \{0\}$ for all $p \in \Omega$ (Adolfo, 2019).

1.3.8 Bifurcation

According to Blanchard et al. (2006), bifurcation is the mathematical study of changes in the qualitative when a small change made to the parameter values of the differential equation. When the vector field is derived depends on a parameter, the structure of the phase space will also depend on this parameter. Thus small changes

may produce no qualitative changes in the phase space until a special value is reached. At this point the phase space change qualitatively and this may change its stability.

The codimension of a bifurcation is the number of parameters which must be varied for the bifurcation to occur, it can be in codimension one bifurcation or codimension two bifurcations (Lyapunov, 1966). Codimension one bifurcation appear to have Hopf (H), Limit Point (LP) and Limit Point of Cycle (LPC). While codimension two bifurcations appear when two parameters varied and this lead to observation of Cusp Point (CP), Bogdanov-Takens (BT), Cusp Bifurcation of Cycles (CPC) and Generalized Hopf (GH) (Kuznetsov and Kuznetsov, 2004).

1.3.8 (a) Codimension One Bifurcation (Curves)

Hopf (H) curve: The location of a Hopf bifurcation on the equilibrium point is characterized by a complex conjugate pair of linear eigenvalues of the Jacobian matrix whose real part passes through zero. When the secondary path is stable or its first Lyapunov coefficient is negative, it becomes the supercritical Hopf bifurcation (sH). Conversely, when the secondary path is unstable or its first Lyapunov coefficient is positive, it becomes the subcritical Hopf bifurcation (uH) (Hale and Kocak, 1991).

Limit Point (LP) curve: Appears when two equilibrium points coalesce and disappear. At this bifurcation point, the Jacobian matrix of the equations at the equilibrium point has a zero eigenvalue (Boeing, 2016).

Limit Point Bifurcation of Cycles (LPC) curve: Appears when two periodic solutions with finite amplitude coalesce and disappear (Lyapunov, 1966).

1.3.8 (b) Codimension Two Bifurcations (Points)

Cusp (CP) point: Appears when two LP bifurcation curves meet and disappear (Boeing, 2016).

Bogdanov-Takens (BT) point: BT point located on the LP curve and the Hopf curve is tangent to the LP curve at this point (Boeing, 2016).

Cusp Bifurcation of Cycles (CPC) point: Appears when two LPC bifurcation curves meet and disappear (Lyapunov, 1966).

Generalized Hopf (GH) point: Appears as a twisted point between uH and sH curves where Hopf bifurcation curve changes its stability at GH point. Each GH is the termination point of the LPC curve tangent to the Hopf curve (Lyapunov, 1966).

1.4 Motivation

Numerical simulation models are required to understand the mechanism of single neuron inside a human brain. Mathematical model that represents phenomenological model needs to be computationally simple and capable of producing periodic firing patterns of AP to exhibit information transmission in real neurons communication mechanism.

The three main motivations emphasized by this research are:

(i) Varied parameters as a means of predictions in certain situations

Neuronal model has been studied in computational neuroscience over the past few decades. In 1952, two physicians, Alan Lloyd Hodgkin and Andrew Fielding Huxley, modelled the dynamics of ion channels that underlie the initial and propagation of AP in neuron via a simple and biophysically realistic model based on data from the squid giant axon (Hodgkin and Huxley, 1952a; 1952b; 1952c; 1952d; Hodgkin et al., 1952). Hodgkin-Huxley (HH) model for AP generation has been applicable for half a century because it is relatively simple and experimentally

testable model which embodies the major features of membrane nonlinearity namely, voltage-dependent ionic currents. The original HH equations not only provide a good model for spike generation and conduction in the squid axon, but also incorporate important features of neuronal excitability, activation and inactivation of voltage-dependent currents. Instead of studying the pattern or mechanism of AP in single neuron, analysing the dynamical systems in single neuron model is more informative in understanding the behaviour of neuron or its bifurcation under varied parameters as a means of predictions in certain situations. HH equation shows a variety of qualitatively different behaviours when the external injection current (I), resting potential of potassium (V_K) and resting potential of sodium (V_{Na}) in HH equations are varied (Fukai et al., 2000a; 2000b). Periodic solutions emerge via Hopf (H) bifurcations, where this analysis of the bifurcation conditions allows us to identify different regimes in the parameter space. This approach of studying bifurcations is useful because it is believed that computational properties of neurons are based on the bifurcations exhibited by these dynamical systems in response to some changing stimulus (Grassia et al., 2012; Doruk, 2017).

(ii) Persuasive discovery in simplified 2-differential model

Experimental and theoretical developments of the past 20 years force HH model practicality to be re-evaluated.

In 1962, FitzHugh and Nagumo reduced 4-differential equations of HH model to 2-differential equations of FitzHugh Nagumo (FHN) model (FitzHugh, 1962; Nagumo et al., 1962). In 2018, a theoretical bifurcation control strategy is presented for FHN model where the bifurcation conditions are tracked by varying membrane potential (V_d) and recovery variable (W) (Doruk and Ihnish, 2018). This paper revealed Hopf (H) and Limit-Point (LP) bifurcation.

In 1981, Catherine Morris and Harold Lecar developed a reduced model named Morris-Lecar (ML) model (Rinzel and Ermentrout, 1998). In 2014, the dynamical behaviours of a Morris–Lecar neuron model presented in one-parameter bifurcation diagrams and pay much attention to the emergence of periodic solutions and bistability by changing injection current (I), fast activation potential (V_1) and slow recovery potential (V_3) (Liu et al., 2014). Bistable systems have an important neurocomputational property where they can be switched from one state to the other by an appropriate stimulation. Bursting oscillations can bring more information compared to normal oscillations, since bursting oscillation carry a bunch of wave signals in one period observation compared to normal oscillation that only carry single signal in periodic waves (Liu et al., 2014).

(iii) Corrective scale for any detected abnormal waves behaviour

In 2000, the dynamics of the HH were explored for a wide range of parameter values in the multiple parameter space and the global structure of bifurcation of the HH determined where parameter plane was divided into several regions according to the qualitative behaviour of equations. The global structure of bifurcations in the multiple-parameter space in the HH suggested that the bistabilities of the periodic solutions are associated with the degenerate Hopf bifurcation points (Fukai et al., 2000a; 2000b). Thus, the study of the behaviour and global structure of bifurcations on this neuronal model become important as a scale guide for each type of wave behaviours.

The studies of dynamical systems for the three neuronal models namely, HH, FHN and ML models in this thesis are based on these three main motivations.